Chapter 3

The Highest Geomagnetic Storms of the Solar Cycle Observed at Ground Level

Carlos E. Navia, Marcel N. de Oliveira and
Carlos R. A. Augusto

Additional information is available at the end of the chapter

http://dx.doi.org/10.5772/intechopen.75688

Abstract

We report two ground-level observations, of geomagnetic storms of different origins; they are among the highest geomagnetic storms, in the solar Cycle 24. The first is St. Patrick's Day storm on March 17, 2015, originated by the impact on Earth's atmosphere of coronal mass ejections (CMEs), the storm reaching the condition of G4 (severe) level, in the NOAA geomagnetic scale. The second included the major geomagnetic storm whose origin is attributed to the interaction with the Earth of a High-Speed Stream (HSS) ahead of a positive polarity coronal hole on October 7, 2015. This storm reached the condition G3 (strong) level. We give emphasis to observations detected by the New-Tupi muon telescopes, located at sea level in Brazil (22.53° S, 43.13° W). We present a study of these observations in correlation with observations reported by multipoint space-based measurements, such as the ACE at Lagrange Point L1 and the geostationary GOES weather satellite, including two global geomagnetic indices and several ground-based detectors. Some considerations on the influence of these geomagnetic storms in the Earth weather are reported.

Keywords: solar physics, geomagnetic storms, space weather, particle detectors

1. Introduction

The previous solar cycle, Solar Cycle 23, peaked in 2000–2002 with many furious solar storms. However, the current solar cycle 24 has not been good to observe geomagnetic storms. Years of weak solar activity have produced few widespread geomagnetic storms [1]. Since its inception, the current solar cycle 24 shows anomalies. March 2008 marked the end of cycle 23 and the beginning of cycle 24 [2]. This means cycle 23 was 11.75 years, higher than the average value of

11 years. In addition, until the second semester of 2010, the sun was in a low level of activity, in an anomalous extended period of minimal solar activity [3].

The current solar cycle 24 had a double maximum of activity [4, 5]; the first happened in late 2013 and another in 2015. In both cases, the solar activity has been relatively low. Now, December 2017, the cycle 24 already is in a declining phase. According to Pesnell from NASA Goddard Space Flight Center, there are similarities between the current cycle 24 and the solar cycle 14, which took place between February 1902 and August 1913 and experienced a double maximum and similar intensity. In addition, the last prediction on Solar Cycle 25 is expected to be the smallest in over 300 years. Suggesting the end of the Modern Warm Period, plummeting Earth into a period of global cooling, which could be like the Mini Ice Age that occurred during the last grand minimum of solar activity, known as the Maunder Minimum [6]. So far, as mentioned earlier, the activity of the solar cycle 24 was weak when compared, for instance, with its predecessor, the cycle 23. The number of geomagnetic storms [7, 8], triggered in each cycle can be used as a comparison between cycles. We have compiled the top 50 geomagnetic storms (using the NOAA weather scales) [9], that is, the 50 strongest geomagnetic storms from Solar Cycle 23 and (so far) on the cycle 24. **Figure 1** show the result of this comparison, where the intensity of a geomagnetic storm is characterized by two indices. The Kp index that indicates the disturbance of the horizontal geomagnetic field and ranging from 0 to 9, a value equal or above 5 indicates the condition of a geomagnetic storm and the G index (NOAA scale for geomagnetic storms), ranging from 1 to 4, G = 1 is equivalent to Kp = 5, and so on.

Following **Figure 1** we can see that the majority (top 50) of the geomagnetic storms on cycle 23 were of type G4 (severe) or Kp = 8, with 22 events. This contrasts with only 6 events (so far) in this category on the cycle 24. In addition, the highest geomagnetic storms, those cataloged as G5 (extreme) or k = 9 on cycle 23, was 13, and none observed in cycle 24. So far, the majority of the top 50 geomagnetic storms on cycle 24 were of type G2 (moderate) or Kp = 6, with 28 events.

The aim of this chapter is to present a global study of the effects on Earth of the highest (so far) geomagnetic storms on the current cycle 24, producing the so-called Forbush decrease (FD) [10–12]. They are defined as sudden decreases of the recorded galactic cosmic ray (GCRs) intensity detected

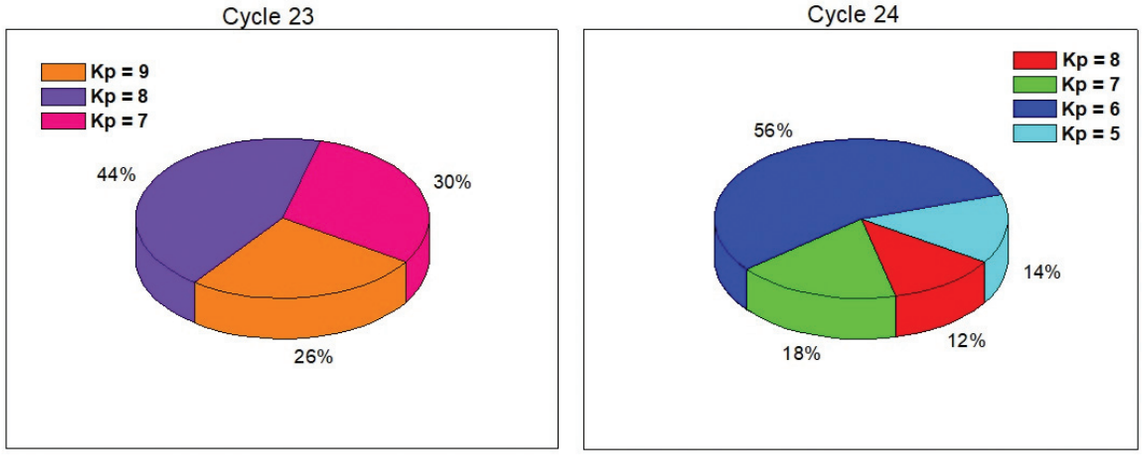

Figure 1. The top 50 geomagnetic storms classified according to Kp index, for Solar Cycle 23 (left panel) and (so far) for the cycle 24 (right panel).

at ground level, followed by a gradual nearly exponential recovery time of several days. The FD are known since long and form an interesting phenomenon. Geomagnetic storms and their ground-level effects can play an important role to understand the global aspects of the weather conditions and is a very active area of research.

The magnitude of FDs observed by a particular detector depends on several factors: the size of the CME, the strength of the magnetic fields in the CME, the proximity of the CME to the Earth, and the location of the detector on the Earth [13]. Initially, this study was limited to three events but a full study is in progress. We compare neutron monitor data and especially the data from the New-Tupi muon telescope with multipoint space-based measurements of the interplanetary space (e.g. ACE/SWEPAM and ACE/MAG and the geostationary GOES weather satellite) and several global geomagnetic indices.

The classification of geomagnetic storms is in two categories: the non-recurrent because the origin is due to the passage of interplanetary counterparts of a coronal mass ejection by Earth. The FD triggered by these geomagnetic storms has a decrease that typically lasts for less than 1 day while the recovery phase may last for several days.

There are also the recurrent geomagnetic storms, whose origins are linked with the interaction with the Earth's magnetic field of a coronal high-speed stream (HSS) [14]. These events dominate near the minimum of the 11-year solar activity cycle. They are recurrent phenomena [15], because, under certain conditions, i.e., stable coronal holes, the HSS can reappear after 27 days, this time is due to Sun rotation period. Even so, they can also appear on and near solar maximum. However, in this case they are less persistent [14]. They are also very important for driving activity in the Earth's magnetosphere, but they are in most cases in minor intensity than the geomagnetic storm originated by CMEs.

The first significant geomagnetic storm of solar cycle 24 was on February 18, 2011. This was the result of the coronal mass ejections ejected on February 14 and 15, 2011. This was also the first significant FD observed from neutron monitors around the world. While the highest geomagnetic storm (so far) was only on March 17, 2015, the so-called St. Patrick Day storm, reaching the condition of a G4 (severe) class, the analysis of this event, considered between the four highest geomagnetic storms of cycle 24, constitute the main core of this article. However, we also have included an analysis of the highest geomagnetic storm whose origin was the interaction with the Earth of a coronal high-speed stream on October 7, 2015. We give emphasis to the observation of the effect at ground level of these three geomagnetic storms through of their FD signatures in different detectors, one of them within the South Atlantic Anomaly (SAA). In this book, we report details of these observations.

2. The New-Tupi detector

The New-Tupi experiment is devoted to the study of cosmic rays and diverse transient events and space weather phenomena in Earth's interplanetary environment. It is an Earth-based apparatus located in the Physics Institute of the Universidade Federal Fluminense, Niteroi, Rio de Janeiro, Brazil (22.53° S, 43.13° W).

The New-Tupi detector is sensitive to primary particles with energies above the pion production threshold (particles with energies around and above GeV scales). The collisions of primary particles, such as the cosmic ray particles or solar energetic particles (ions) with atmospheric nuclei produce secondary particles; the most abundant are the pions (subatomic particle). The pions decay into muons and neutrinos. Muons reach the ground level and are detected by a variety of apparatus placed on the surface of the Earth and underground. The New-Tupi detector consists of four particle detectors. The four detectors are placed in pairs forming three telescopes. This configuration is able to measure the muon flux (coincidence rate between two detectors) from three directions: the vertical (zenith), west and east (with an inclination of 45°). The separation between the detectors (vertical and horizontal) is 2.83 m. Details of the New-Tupi detector can be found in [16].

The New-Tupi detector is within the South Atlantic Anomaly (SAA) region. This region is characterized by an anomalously weak geomagnetic field strength (less than 28,000 nT). It is in the SAA region where the inner Van Allen radiation belt makes its closest approach to the Earth's surface. This behavior of the magnetosphere is responsible for several processes, such as the high conductivity of the atmospheric layers due to the precipitation of energetic trapped particles from the inner Van Allen belt.

3. The St. Patrick's day storm

Two days before St Patrick's Day, on March 15, 2015, the sunspot 2297 produced a C9.1 class flare with onset at 01:15 UT and peaking at 02:13 UT. Indeed, a C-Flare does not draw attention because they are relatively common solar explosions. However, in this case, the blast was of long duration, beyond 2 hours and the active area was located at west of the solar disk (S22, W29), that is, in a geo-effective location. In addition, the blast triggered a partial halo coronal mass ejection (CME) toward the earth. The Solar Dynamics Observatory (SDO) [17] using the 94 angstroms channel has shown the explosion and it is reproduced in **Figure 2** (left panel), and the register of the CME by Cactus C2 Lasco is reproduced in **Figure 2** (right panel).

The detection of Type II and Type IV radio emission [18] was the indication of the presence of CME shocks, they are typically associated with strong coronal mass ejections and solar radiation storms. Indeed, the blast triggered a solar radiation storm, that is, solar energetic particles (SEP) began to flow around the planet at early hours, on March 15, 2015, on a gradual rise, reaching the condition of an almost S1 (minor) radiation storm in the NOAA scale on March 16. There was a small and narrow enhancement of the counting rate at the vertical New-Tupi telescope, in association with the SEP peak, as observed by ACE-SIS at L1 Lagrange point, as well as at GOES. **Figure 3** summarizes the situation.

According to WSA-ENLIL SOLAR WIND PREDICTION, the impact of the CME with the Earth's atmosphere would be only on March 18, 2015, triggering a geomagnetic storm of only G1 (minor) level of intensity. However, at 04:05 UTC on March 17, 2015, 15 hours earlier than expected, the ACE spacecraft detected the passage of a shock wave. In addition, the Bz component of the interplanetary magnetic field (IMF) was initially pointing north, but through

http://dx.doi.org/10.5772/intechopen.75688

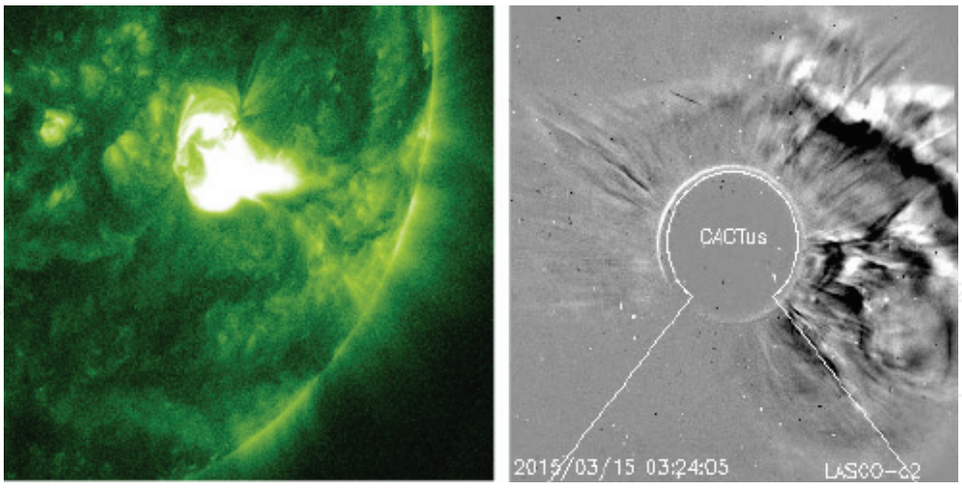

Figure 2. Left panel: Register of the long duration C9.1 peaking at 02:13 UT (March 15, 2015) around sunspot 2297. Credit: SDO/AIA. Right panel: Register of the partial CME associated to the C9.1 are. Credit: C2 Lasco.

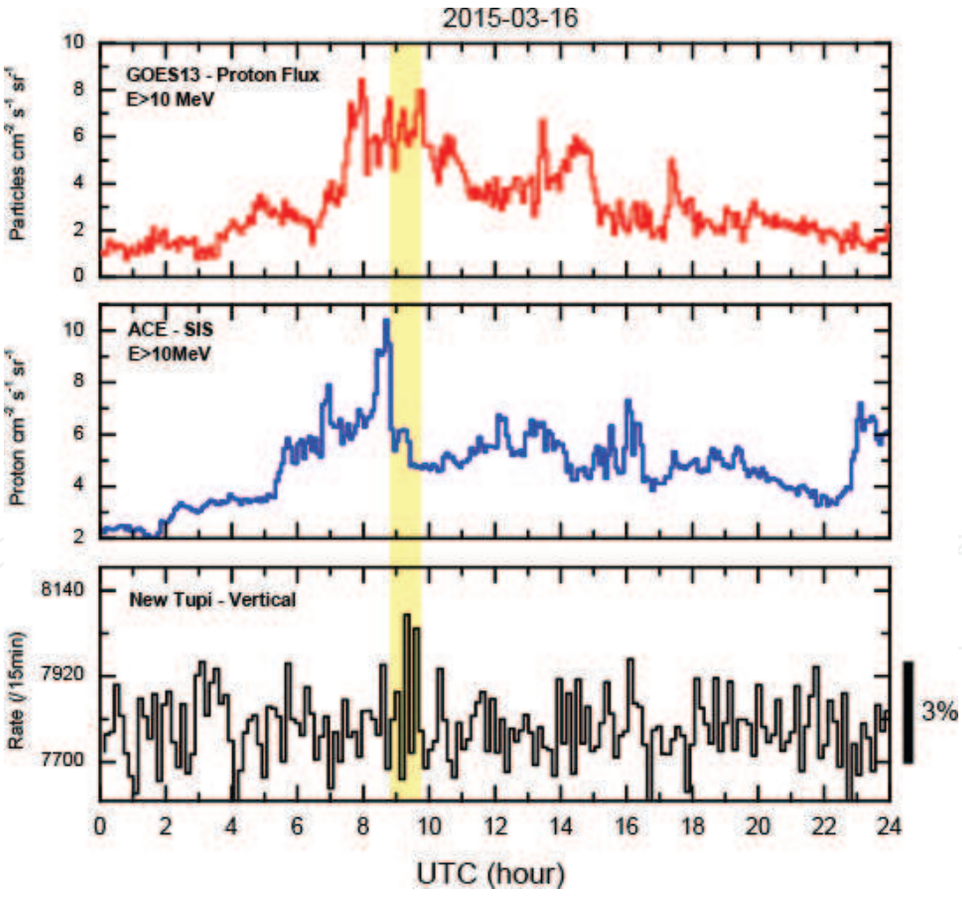

Figure 3. Time profiles observed in three different detectors on March 16, 2015. Top panel: the proton flux with energies above 10 MeV, according to the geostationary weather satellite. Central panel: the proton flux with energies above 10 MeV at Lagrange point L1, according to SIS instrument at ACE spacecraft. Bottom panel: the muon counting rate 15 minute binned, according to the vertical New-Tupi telescope.

a fast oscillation it finished pointing to the south with a maximum magnetic field (Bz) of −30 nT (−20 nT sustained). Then began a period of enhanced geomagnetic activity reaching G3 (strong) to G4 (severe) geomagnetic conditions and sustained for 12 hours, as shown in **Figure 4** (left top panel), where the time profiles of the interplanetary magnetic field Bt and Bz component are shown. Solar wind speeds as measured by ACE spacecraft increased to above 500 km/s, reaching up to a maximum wind speed of 680 km/sec, as shown in **Figure 4** (left central panel), where the effects of the CME on the solar wind at Lagrange point L1 is shown.

The arrival of the shock wave on Earth was 33 minutes after its passage through the Lagrange point L1, because there is the register at 04:35 UT of a geomagnetic sudden impulse measuring 54 nT by the USGS ground-based magnetometer in Boulder, Colorado. This signaled the moment the interplanetary shock wave (coronal mass ejection) swept past the Earth.

The bottom panel of **Figure 4** shows the register of the counting rate in two different instruments, New-Tupi detector, and Nain NM. Despite both being in different locations and consequently having different geomagnetic conditions, because the Nain NM is located at high latitude, close to the North Pole, their counting rates show a correlation. The FD intensity (changing in the counting rate) in New-Tupi was 2.5%, whereas in Nain was 3.8%. In addition, it is possible to see that the onset of FD observed at the muon counting rate in the New-Tupi telescope (and at the Nain NM) are in correlation with the onset of the geomagnetic storm.

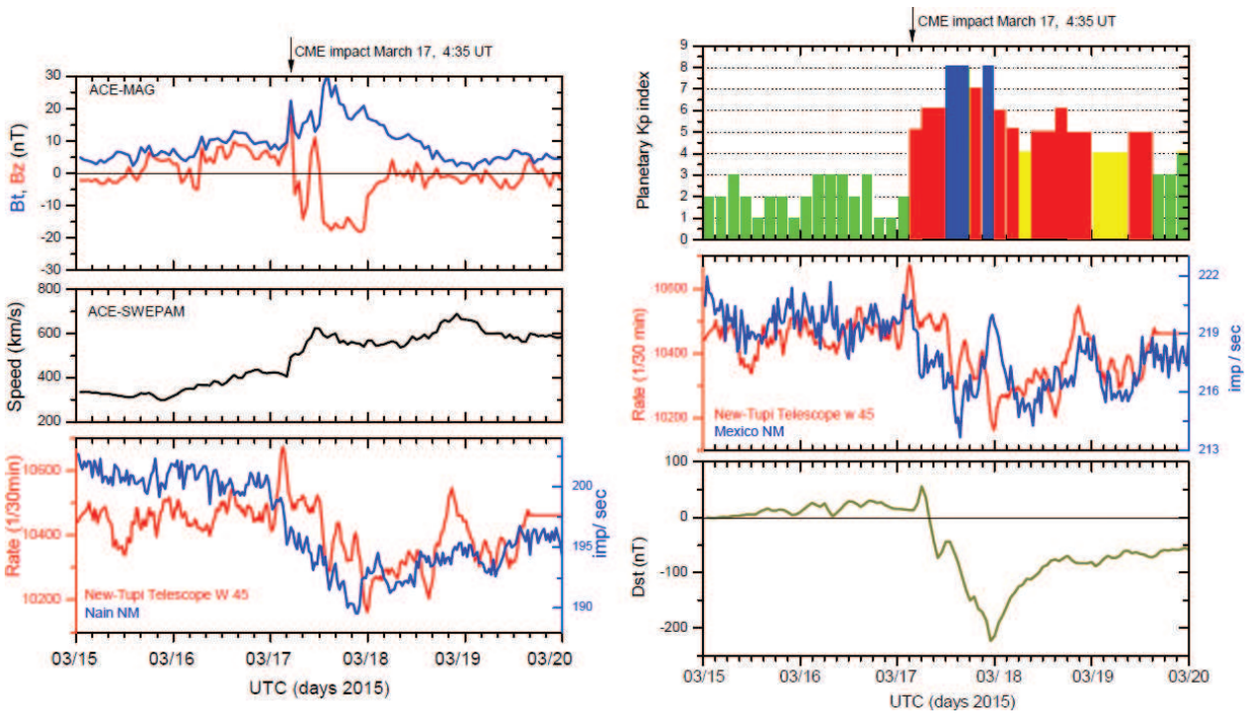

Figure 4. (Figures on the left) Top and central panels: the time profiles of the solar wind magnetic field components Bz and Bt and the solar wind speed, respectively, observed by the ACE spacecraft. Bottom panel: the 30 minutes muon counting rate in the New-Tupi mu telescope and Nain NM. (Figures on the right) Top panel: the time profiles of the geomagnetic planetary Kp index. Central panel: the 30 minutes muon counting rate in the New-Tupi muon telescope and Mexico NM. Bottom panel: the time profiles of the geomagnetic Dst index. In all cases, the time profiles are in the period from on March 15–19, 2015.

These signatures can be seen through the time profiles of the magnetic field, Bz, component (top panel) as well as with the solar wind speed increase (central panel).

The CME's impact on Earth triggered a G4 level (severe) (or Kp = 8) geomagnetic storm with onset about 14:00 UT on March 17, 2015, as is shown in the right top panel in **Figure 4**. The geomagnetic storm had a duration of about 18 hours, with a G3/G4 condition sustained for 12 hours. The right central panel in **Figure 4** shows also a good correlation between the time profiles of the Kp index and the counting rate in New-Tupi detector; in this case, we have included also, for comparison, the counting rate in Mexico NM. Finally, in the right bottom panel in **Figure 4** we have included the time profiles of the Dst index, based on the ring current around Earth produced by solar electrons and protons. They induce a magnetic field opposite Earth's magnetic field. During a geomagnetic storm, this induced magnetic field is higher than the Earth's geomagnetic field, and the resulting magnetic field is negative.

So far, this was the strongest G4 storm of Solar Cycle 24, known as the St. Patrick's Day storm.

4. The high-speed stream on October 7, 2015

Geomagnetic storms, at least the most intense, are generally the result of Coronal Mass Ejections intersecting with the Earth. However, coronal holes are the most common source of geomagnetic storms. Coronal holes occur when the Sun's magnetic field is open to interplanetary space; they are seen as a large dark region, and this characteristic is a consequence of being in colder regions. The open configuration of the magnetic field in coronal holes allows the particles to escape from the solar corona. Thus, they are sources of high-speed solar wind streams. Thus, when the coronal hole is geo-effective, that is, located near the Sun's central region, its associated HSS can reach the Earth's magnetosphere; under this condition there is an efficient exchange of energy from the high-speed solar wind to the magnetosphere, producing a disturbance on it.

An equatorial coronal hole high speed stream (HSS), with positive polarity flowed on 6 October 2015, could be seen in the SDO images, such as shown in **Figure 5**.

The HSS plasma flows following the spirals of the interplanetary magnetic field lines, forming a stream interaction region (SIR) at the compressed boundary between the fast and slow wind. **Figure 6** shows a schematic of this configuration, where an HSS with the southward interplanetary magnetic field sets up the interplanetary electric field $E = -V_{IMF} \times B$. The Parker spiral has a minor influence on the HSS than on the slower solar wind speed.

We would like to point out that on October 7, 2015 two coincident phenomena occurred; both contributed to the enhancement of the geomagnetic storm on October 7, 2015.

The first was the crossing of Earth for the Heliospheric Current Sheet (HCS), as represented in the top panel of **Figure 7**; it gives a snapshot of the WSA-Enlil model, run around on October 7, 2015 [16, 19, 20]. The model shows the solar wind plasma density in the ecliptic plane. Green to red colors show very high plasma density and blue color represents low density. A HCS is a

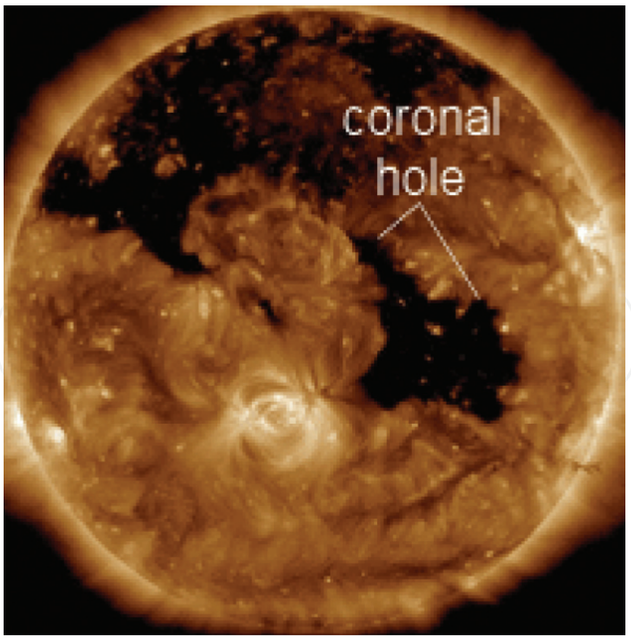

Figure 5. The sun equatorial coronal hole that gave origin to a high-speed stream (HSS), with positive polarity flowed on October 6, 2015. Credit: C2 SDO/AIA.

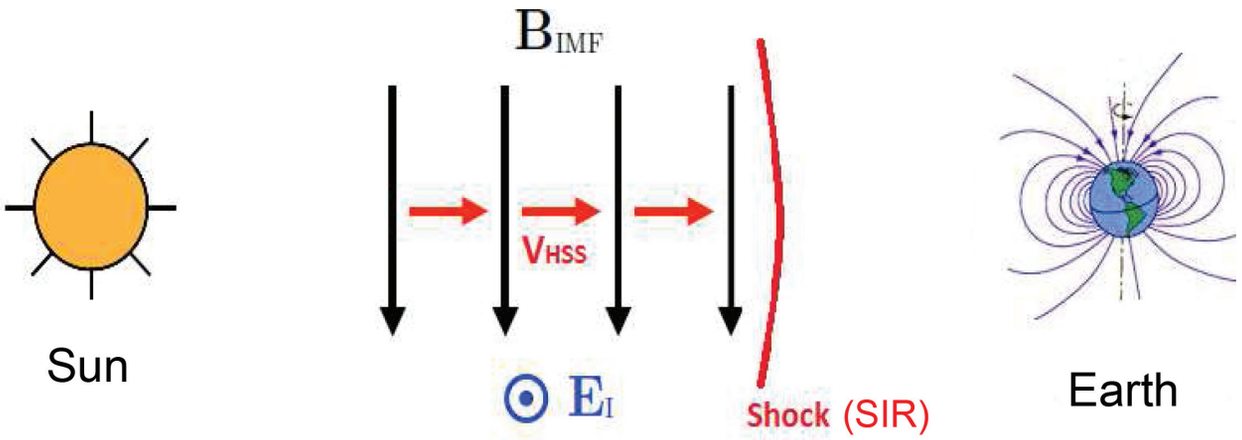

Figure 6. Schematic image of the high-speed stream approaching the Earth magnetosphere. The arrows pointing downwards represent the interplanetary magnetic field. In this configuration, an electric field E (open circle with dot) points out from the plane. The rightward arrows represent the solar wind speed. The arc line indicates a stream interaction region (SIR) forward shock.

transition zone that separates regions of opposing interplanetary magnetic field polarity [21]. An increase in the density of plasma concentration and of the interplanetary magnetic field (IMF) intensity is associated with the HCS compression region. This means that the HCS plays a magnetic focusing role to charged particles; they propagate more efficiently following the HCS sectors. In some cases, the crossing of Earth by HCS also can propitious a small enhancement in galactic cosmic ray (GCR) flux observed at ground level, as shown by [22].The Earth is marked as the green circle, and the Sun by the yellow circle. Following this figure, we can see

http://dx.doi.org/10.5772/intechopen.75688

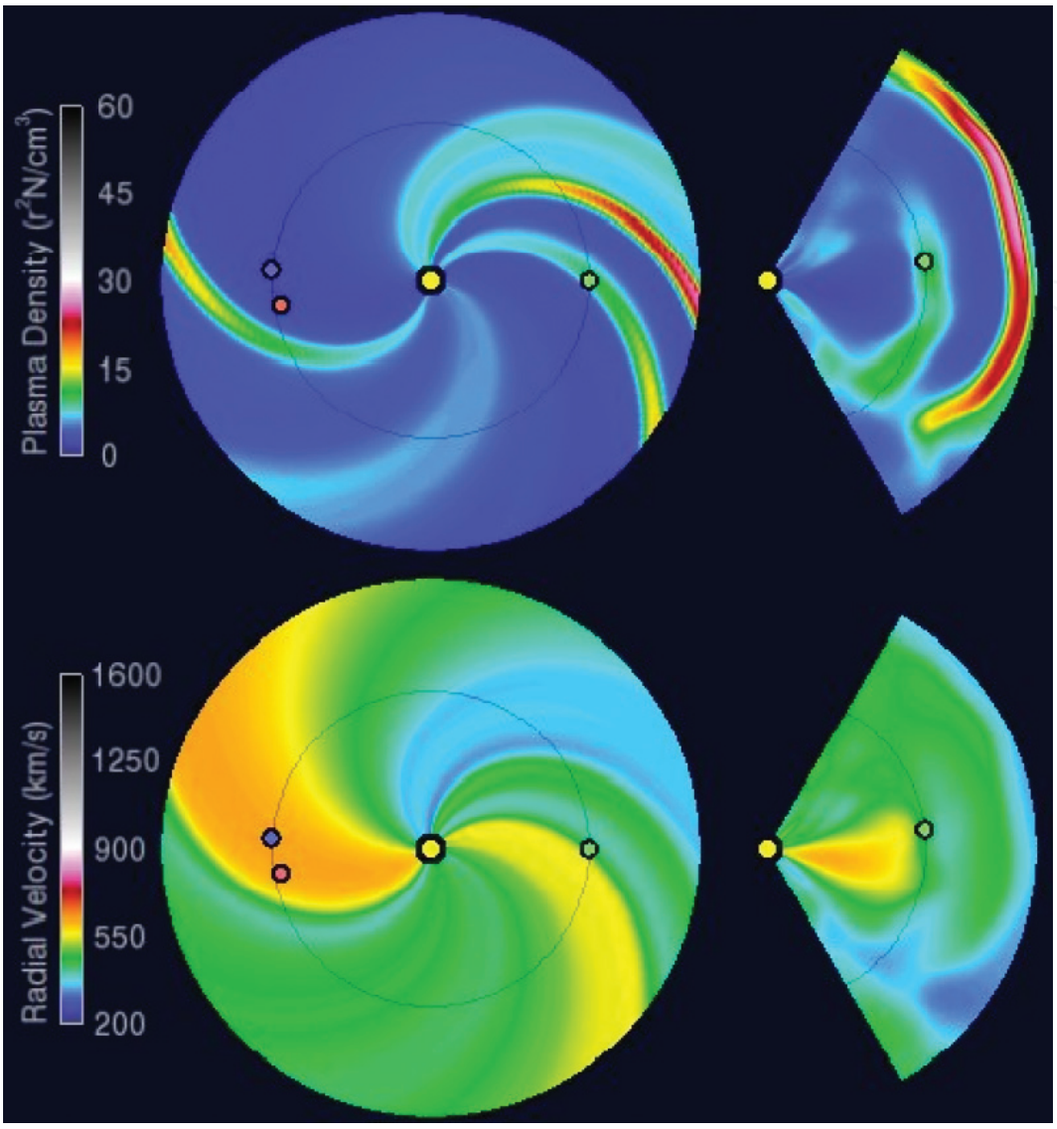

Figure 7. Top panel: Solar wind particle density and bottom panel: the solar wind speed gradients, according to the WSA-Enlil model. The central circle represents the Sun and the circle at the right represents the Earth on October 7, 2015.

that on 7 October the Earth was crossing a narrow region of high solar plasma density, that is, crossing the HCS.

The second was that at early hours of October 7, 2015, the Earth entered a region of a high-speed stream from a positive polarity coronal hole, as provided by the WSA-Enlil Solar Wind Prediction model and shown in the bottom panel in **Figure 7**. The long large-scale plasma structure, generated by the interaction of a stable fast solar wind stream, with the surrounding slow solar wind is called as corotating interaction region (CIR) [23]. The generation of forward and reverse magnetic shocks in the boundary regions of the CIR can accelerate ions from MeV to GeV energies. In addition, the magnetic perturbation of the magnetosphere due to the impact of the HSS can act as shadow effect to the galactic cosmic rays, producing an FD at ground-level detectors. Thus, the HSS impact on the magnetosphere on 7 October had the influence to start a period of an active geomagnetic storm.

The first signal of the HSS was at early hours, about 02:00 UTC at Lagrange Point L1, the interplanetary magnetic field had an enhancement of around twice its previous value, as shown in the ACE-MAGNETIC and reproduced in **Figure 8** (top left panel). Simultaneously, the Bz component had a southward deviation. In addition, the solar wind speed had a fast rise from 400 km/s to above 700 km/s and reproduced in **Figure 8** (central left panel). These were the signatures of an interplanetary shock wave due to the passage of HSS by the Lagrange Point L1.

In almost temporal coincidence with the fast rise of the solar wind speed at ~12:00 UT, there was a fast falling in the counting rate (FD) of the New-Tupi telescope that pointed to the west, with a confidence about 2.5%; the result is in **Figure 8** (bottom left panel). As predicted, the effect at Earth was a geomagnetic storm with onset at early hours on 7 October, reaching the condition of G3(strong) or Kp = 7 as shown in **Figure 8** (top right panel). It was a geomagnetic storm of relatively long duration, covering October 7 and 8 with a G2/G1 (Kp = 6/Kp = 5) conditions, sustained for more of 21 hours.

In addition, from **Figure 8** we can see that the FD observed in the muon counting rate of New-Tupi telescope (central right panel) was with a confidence of 2.5%. It is correlated with the geomagnetic storm, whose signature at Earth can be seen through the time profiles of the planetary Kp index (top right panel). As well as in the Dst index time profiles (bottom right

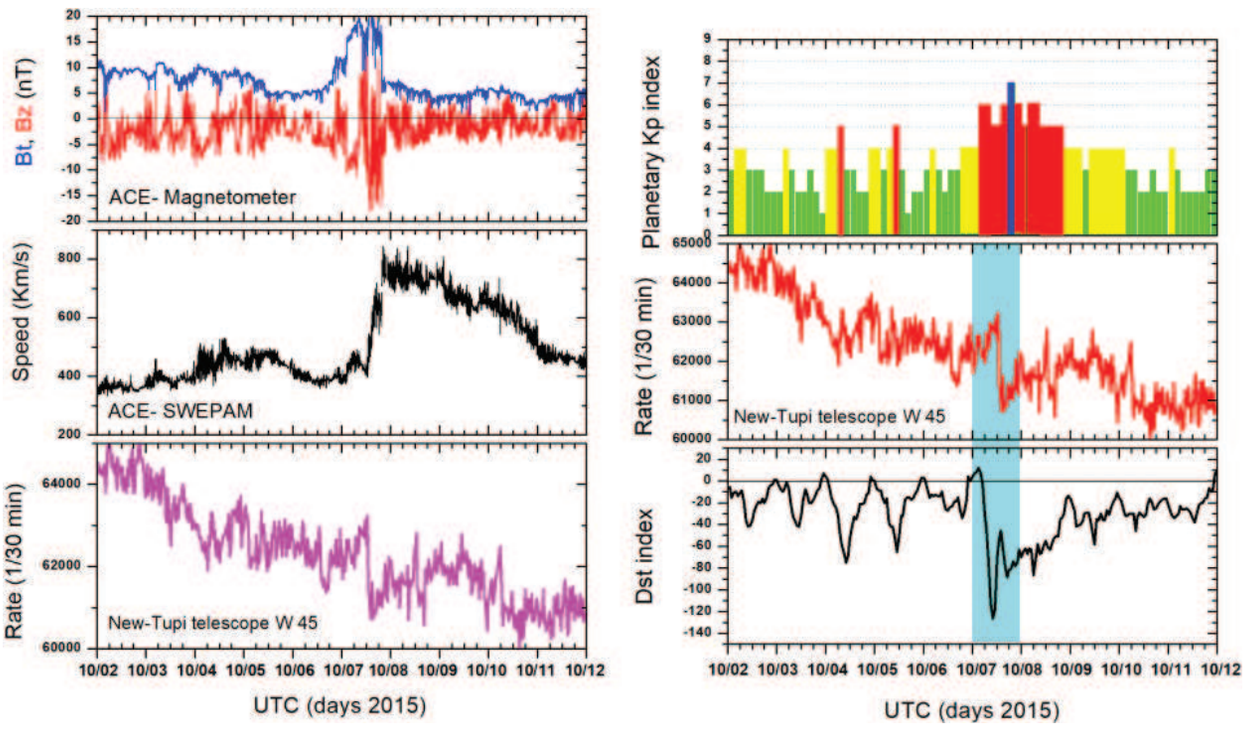

Figure 8. (Figures on the left) Top and central panels: the time profiles of the solar wind magnetic field components Bz and Bt and the solar wind speed, respectively, observed by the ACE spacecraft. Bottom panel: the 30 minutes muon counting rate in the New-Tupi muon telescope. (Figures on the right) Top panel: the time profiles of the geomagnetic planetary Kp index. Central panel: the 30 minutes muon counting rate in the New-Tupi muon telescope. Bottom panel the time profiles of the geomagnetic Dst index. In all cases, the time profiles are in the period from on October 2–12, 2015.

panel). Notice that the fast fall at New-Tupi coincides with the minimum Dst value, reaching a value of about −120 nT.

We would like to point out, that a similar behavior, such as the one observed at New-Tupi also was observed in the counting rate of the South Pole NM. However, in most NMs, the fall in the counting rate does not present a clear FD. In most cases it is only a fall smaller than 1.5% and with a recovery time less than 6 hours.

5. Impact of solar activity in the terrestrial climate

5.1. Incidence of electromagnetic radiation

The principal source of energy on Earth is the Sun. The radiated energy by the Sun covers all electromagnetic spectrum. However, the radiation on the range of the visible spectrum (wavelengths around 400–800 nm) has the most contribution. The Sun's visible radiation at Earth (distance of 1-AU) is nearly constant, and the main variation of around 0.1% follows the 11-year solar cycle progression. The total wavelength-integrated energy from sunlight at Earth is known as the Solar Constant (SC) or Total Solar Irradiance (TSI) whose value vary from 1365.5 Watts/m^2 at solar minimum to 1366.5 Watts/m^2 at solar maximum.

There is also a minor contribution of the energy irradiated by the Sun in other wavelengths of the electromagnetic spectrum, such as the Ultraviolet (UV) (wavelengths around 120–400 nm), the X-rays and gamma radiations. The radiations with wavelengths smaller than the wavelength of visible radiation are absorbed in the upper atmosphere, for instance, a large fraction of UV radiation is absorbed by ozone in the stratosphere. The gamma and X-ray radiations have large variability of up to 300% over very short timescales (e.g., several minutes). This large variability is associated with solar transient events such as flares. These radiations in short wavelength have minimal impact on the Earth weather.

On the other hand, in wavelengths smaller than the visible spectrum, there is also a minor contribution, such as the Infrared (IR) (wavelengths 800–10,000 nm) with small changes of up to 1% over the solar cycle progression. Finally the solar radio waves, they are a transient contribution linked to the solar flares and they are called Radio Blackouts (RB). Depending on the solar flare intensity, RB can cover a wide area blackout of HF radio communication, loss of radio contact with duration of up to hours on the sunlit side of Earth and the degradation of Low-frequency navigation signals with a duration of up to hours.

5.2. Incidence of solar particles

The Earth geomagnetic field is a natural shielding to charged particles coming from space; low-energy particles are largely deflected when their incidence is near equatorial regions. However, the deflection is lower near Polar Regions or above roughly 55° of latitude.

In addition, the Sun is also the source of e Solar Energetic Particles (SEP) accelerated up to GeV energies during the occurrence of solar flares and CMEs. In space weather physics, these

particles are the so-called radiation storms. If the solar active region is close to the central meridian (i.e., geo-effective region), the SEP can reach the Earth. The S1 level of a radiation storm indicates that the flux of protons at 1-AU with energies above 10 MeV equals or exceeds 10 pfu (1 pfu = 1 particle per cm^2 s sr). The scale is logarithmic, this means that 100 pfu indicate an S2 level, and so on.

Under certain conditions, SEP can penetrate into the magnetosphere and reach the upper and middle atmosphere. This behavior can have long lasting consequences, such as the changes in the concentration of some molecules as the NOx species [24]. However, the influence of these changes in the Earth weather is not yet clear.

5.3. Incidence of galactic cosmic rays

The interplanetary magnetic field (IMF) is modulated by the solar cycle; the maximum activity solar occurs every 11 years and it is when the Sun's magnetic field inverts its polarity and shuffles the IMF. This behavior modulates the lower energy component of the galactic cosmic rays (GCR), that is, the ∼11-year variation in cosmic ray intensity observed at the Earth is anti-correlated with solar activity. The almost isotropic flux of GCR when they enter the heliosphere is modified, around the solar maximum activity, their dispersion is higher, and this reduces the incidence of cosmic rays flux on the Earth. In addition, around the minimum solar activity, the Sun's magnetic field has a defined polarity and the cosmic rays dispersion is lower; consequently, the incidence of cosmic rays flux on the Earth is higher.

Thus, at solar minimum, the number of cosmic rays reaching Earth increases. These cosmic ray particles can be the source for creating nucleation sites in the atmosphere, that is, the seed of nucleation in cloud formation and create rain conditions [25]. In other words, the impact on Earth weather conditions can be modulated by the 11-year solar cycle. This topic needs further studies.

5.4. Injection of accelerated particles by an interplanetary shock

According to satellite observations, such as the NASA's IMAGE spacecraft and the joint NASA/European Space Agency Cluster satellites, immense cracks sometimes develop in Earth's magnetosphere and remain open for hours due to magnetic reconnection.

In the Earth, the magnetic reconnection is a phenomenon that occurs in several situations, in all cases, a high-speed magnetized plasma, reach a region of the magnetosphere with an oppositely directed magnetic field, the components break and there is a cross-connect, forming a crack in the magnetosphere, transferring the energy stored in the magnetic fields to plasma motion and heat.

Reconnection can occur between Earth's magnetic field and the interplanetary magnetic field (IMF) carried by a coronal mass ejection or a high-speed stream, emanating from the sun. Reconnection occurs at the boundary of Earth's magnetosphere, the region of space that is dominated by Earth's magnetic field. However, despite some models predicting the properties of reconnection at this boundary, there are some issues, which are poorly understood, such as, where reconnection really occurs.

The model with a southward interplanetary magnetic field leads to a natural explanation of neutral points of the geomagnetic field [26]. A number of methods have been developed to locate magnetic separators, that is, the location where B = 0, such as the magnetic nulls in global magnetospheric simulations [27] that allow determining the separator for both northward and southward IMF orientations [28].

The first point of reconnection is in the day-side of Earth (left point in **Figure 9**) where a crack opens in the magnetic shield and remains open for hours, through which the electrically charged particles from space can flow. This includes particles from high-speed solar wind, particles accelerated in the front of the shock wave and up to galactic cosmic rays of low energy.

There is also reconnection in the magneto-tail results in a cross-tail electric field, in the night-side of Earth (right point in **Figure 9**). The electric field generated by this reconnection process directs the plasma injected by the crack due to the reconnection in the day-side, again to the Earthward.

At about three times of the Earth radii, the ions and electrons begin drifting in different directions around the Earth; in the geomagnetic equatorial plane, the positive ions drift westward, and the electrons drift eastward. This charge separation creates the ring current J_{DST}. The ring current around Earth produces a magnetic field B_{DST} that is directly opposite the Earth's magnetic field and generates the so-called Dst index. A negative Dst value means that Earth's magnetic field is weakened. This is particularly the case during solar magnetic storms.

Recent results [16] show some evidences of a particle injection into the Earth atmosphere, driven by the HSS on August 28, 2015, as shown in **Figure 10**. In the top panel we show the time profiles of the New-Tupi muon counting rate, the central and bottom panels show the time profiles of the solar wind speed and particle density in the ACE spacecraft, respectively. The impact of HSS (shock arrival) occurred when the magnetosphere was already disturbed by the impact of a previous CME on October 25, 2015, triggering a geomagnetic storm and a FD that was already underway.

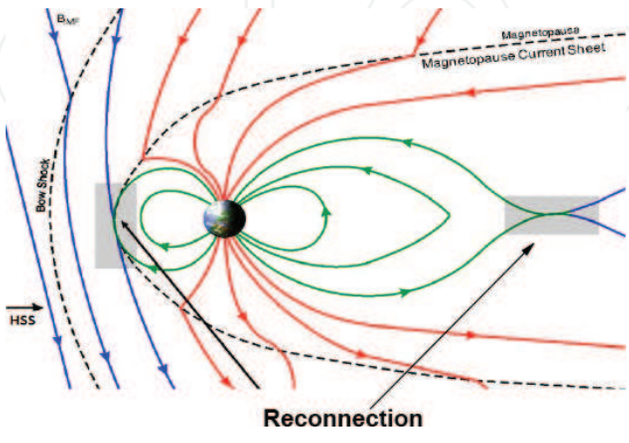

Figure 9. Schematic view of the magnetic reconnection in the Earth's magnetosphere. The black arrows indicate where magnetic reconnection occurs.

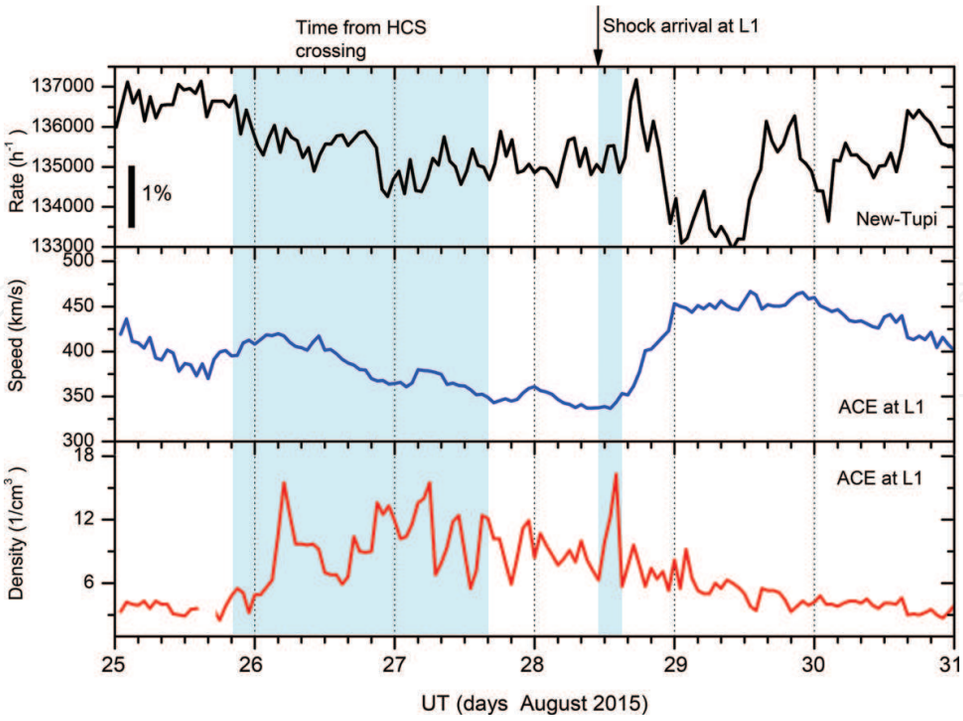

Figure 10. Comparison between the muon counting rate in the New-Tupi telescope (top panel) and the solar wind parameters (density and speed) observed by the ACE satellite (center and bottom panels) in the period from August 25 until August 31. The shaded area indicates the HCS crossing time and the vertical arrow show the arrival of a shock associated with a high-speed stream on August 28.

The energy of the injected particles reached up to GeV values because from their interactions in the upper atmosphere, muons were produced and a fraction of them reached the ground level. In most cases, these injected particles are directed to the Polar Regions. However, the particles from the high-energy tail of the spectrum can reach mid-latitudes. The injected energy in the upper atmosphere during the HSS impact had a duration of ~350 minutes and a value above 1.4×10^{-4} erg per cm^2. This behavior could have consequences for the atmospheric chemistry. For instance, the creation of NOx species may be enhanced, and this can lead to increased ozone depletion [24]. This topic requires further study.

6. Conclusion(s)

Space magnetic conditions in the interplanetary medium and consequently within the Earth's magnetic environment are constantly influenced by the transient disturbances in the interplanetary medium propagating from the Sun, such as CMEs and HSSs. We have presented here two examples of these events producing magnetic disturbances known as geomagnetic storms.

The first is one of the highest geomagnetic storms in the current solar cycle 24, on March 17, 2015 (St. Patrick's Day) and it reached the condition of G4 (Kp = 8) in the NOAA storm scale. The origin was a CME impact, consequently. The second was the impact of an HSS on October

7, 2015, whose origin was a positive coronal hole. In both cases, the passage of these two events by L1 had an interplanetary shock signature, with a fast rising of the solar wind. The effect at ground level was an FD; however, it is possible to see (especially in the first event) some particle enhancements. The probable origin of these particles' enhancement is the anisotropies in the perturbed Earth magnetic field, the magnetic reconnection between the magnetic field of the interplanetary shock and the geomagnetic field, opening cracks in the Earth magnetic shield (please see Section 5).

In order to see better the particle injection in the upper atmosphere, we show a prolonged energetic (in the GeV energy scale) particle injection within the Earth atmosphere system, driven by an HSS on August 28, 2015.

This mechanism could be correlated with the renovation of the atmospheric chemistry. In addition, the formation of NOx species can be enhanced and can be correlated with the ozone depletion and abundance [24]. This mechanism correlates with the atmospheric chemistry requires further study.

Acknowledgements

The support from National Council Research (CNPq) and Fundação de Amparo a Pesquisa do Estado do Rio de Janeiro (FAPERJ) both in Brazil is gratefully acknowledged. We express our thanks to the ACE/MAG instrument team, the ACE Science Center, the NASA GOES team and the NOAA Space Weather Prediction Center (www.swpc.noaa.gov), the Geomagnetism at Kyoto University, Japan (wdc.kugi.kyoto-u.ac.jp) and the NMDB database (www.nmdb.eu), founded under the European Union's FP7 program (contract no. 213007), for providing real time data. We also express our gratitude to V. Kopenkin and A. Nepomuceno for valuable discussions and their help.

Author details

Carlos E. Navia*, Marcel N. de Oliveira and Carlos R. A. Augusto

*Address all correspondence to: tupi.carlos24@gmail.com

Instituto de Física, Universidade Federal Fluminense, Rio de Janeiro, Brazil

References

[1] Rezaei R, Schmidt W, Beck C. Comparison of sunspot properties in cycles 23 and 24. In: 40th COSPAR Scientific Assembly. 2014;**40**:E2.4-15-14. ADS: 2014cosp…40E2740R

[2] Basu S. The peculiar solar cycle 24–where do we stand? Journal of Physics: Conference Series. IOP Publishing. 2013;**440**:012001. DOI: 10.1088/1742-6596/440/1/012001

[3] Abdo A, Ackermann M, Ajello M, Baldini L, Ballet J, Barbiellini G, et al. Fermi large area telescope observations of two gamma-ray emission components from the quiescent sun. The Astrophysical Journal. 2011;**734**(2):116. DOI: 10.1088/0004-637X/734/2/116

[4] Hathaway DH. The solar cycle. Living Reviews in Solar Physics. 2015;**12**:4. DOI: 10.1007/lrsp-2015-4

[5] Gonzalez WD, Gonzalez AC, Tsurutani BT. Dual-peak solar cycle distribution of intense geomagnetic storms. Planetary and Space Science. 1990;**38**(2):181. DOI: 10.1016/0032-0633(90)90082-2

[6] Vaquero JM, Kovaltsov GA, Usoskin IG, Carrasco VMS, Gallego MC. Level and length of cyclic solar activity during the maunder minimum as deduced from the active-day statistics. A&A. 2015;**577**:A71. DOI: 10.1051/0004-6361/201525962

[7] Gonzalez WD, Joselyn JA, Kamide Y, Kroehl HW, Rostoker G, Tsurutani BT, Vasyliunas VM. What is a geomagnetic storm? Journal of Geophysical Research. 1994;**99**:5771. DOI: 10.1029/93JA02867

[8] Augusto CRA, Kopenkin V, Navia CE, Tsui KH, Shigueoka H, Fauth AC, et al. Variations of the muon flux at sea level associated with interplanetary ICMEs and corotating interaction regions. The Astrophysical Journal. 2012;**759**:143. DOI: 10.1088/0004-637X/759/2/143

[9] NOAA / NWS Space Weather Prediction Center. NOAA Space Weather Scales [Internet]. 2018. Available from: http://www.swpc.noaa.gov/sites/default/files/images/NOAAscales.pdf [Accessed: 26-January-2018]

[10] Forbush SE. On the effects in cosmic-ray intensity observed during the recent magnetic storm. Physics Review. 1937;**51**(12):1108. DOI: 10.1103/PhysRev.51.1108.3

[11] Cane HV. Coronal mass ejections and Forbush decreases. In: Cosmic Rays and Earth. Space Science Reviews. 2000;**93**:55. DOI: 10.1023/A:1026532125747

[12] Lockwood JA, Webber WR, Debrunner H. Forbush decreases and interplanetary magnetic field disturbances: Association with magnetic clouds. Journal of Geophysical Research. 1991;**96**(A7):11587. DOI: 10.1029/91JA01012

[13] Belov A, Abunin A, Abunina M, Eroshenko E, Oleneva V, Yanke V, et al. Coronal mass ejections and non-recurrent Forbush decreases. Solar Physics. 2014;**289**:3949. DOI: 10.1007/s11207-014-0534-6

[14] Kavanagh A, Denton M. High-speed solar-wind streams and geospace interactions. Astronomy & Geophysics. 2007;**48**:6.24. DOI: 10.1111/j.1468-4004.2007.48624.x

[15] Tsurutani BT, Gonzalez WD, Gonzalez AL, Guarnieri FL, Gopalswamy N, Grande M, et al. Corotating solar wind streams and recurrent geomagnetic activity: A review. Journal of Geophysical Research. 2006;**111**(A7). DOI: 10.1029/2005JA011273

[16] Augusto CRA, Navia CE, de Oliveira MN, Nepomuceno AA, Kopenkin V, Sinzi T. Muon excess at sea level during the progress of a geomagnetic storm and high-speed stream

impact near the time of Earth's Heliospheric sheet crossing. Solar Physics 2017;**292**:107. DOI: 10.1007/s11207-017-1116-1

[17] Lemen JR, Title AM, Akin DJ, et al. The atmospheric imaging assembly (AIA) on the solar dynamics observatory (SDO). Solar Physics. 2012;**275**:17. DOI: 0.1007%2Fs11207-011-9776-8

[18] Stewart RT, Sheridan KV. Evidence of type II and type IV solar radio emission from a common flare-induced shock wave. Solar Physics. 1970;**12**:229. DOI: 10.1007/BF00227120

[19] Odstrcil D, Smith Z, Dryer M. Distortion of the heliospheric plasma sheet by interplanetary shocks. Geophysical Research Letters. 1996;**23**:2521. DOI: 10.1029/96GL00159

[20] Odstrcil D. Modeling 3-D solar wind structure. Advances in Space Research. 2003;**32**:497. DOI: 10.1016/S0273-1177(03)00332-6

[21] Wilcox JM, Ness NF. Quasi-stationary corotating structure in the interplanetary medium. Journal of Geophysical Research. 1965;**70**(23):5793. DOI: 10.1029/JZ070i023p05793

[22] Thomas SR, Owens MJ, Lockwood M, Scott CJ. Galactic cosmic ray modulation near the heliospheric current sheet. Solar Physics. 2014;**289**(7):2653. DOI: 10.1007/s11207-014-0493-y

[23] Pizzo V. A three-dimensional model of corotating streams in the solar wind. Journal of Geophysical Research. 1978;**83**(A12):5563. DOI: 10.1029/JA083iA12p05563

[24] Seppala A, Verronen PT, Clilverd MA, Randall CE, Tamminen J, Soeva V, Kyrolo E. Arctic and Antarctic polar winter NOx and energetic particle precipitation in 2002–2006. Geophysical Research Letters. 2007;**34**:L12810. DOI: 10.1029/2007GL029733

[25] Kirkby J, Curtius J, Almeida J, Dunne E, Duplissy J, Ehrhart S, et al. Role of sulphuric acid, ammonia and galactic cosmic rays in atmospheric aerosol nucleation. Nature. 2011;**476**(7361): 429. DOI: 10.1038/nature10343

[26] Dungey JW. Interplanetary magnetic field and the auroral zones. Physical Review Letters. 1961;**6**(2):47. DOI: 10.1103/PhysRevLett.6.47

[27] Dorelli JC, Bhattacharjee A, Raeder J. Separator reconnection at Earth's day-side magnetopause under generic northward interplanetary magnetic field conditions. Journal of Geophysical Research. 2007;**112**:A02202. DOI: 10.1029/2006JA011877

[28] Hu YQ, Peng Z, Wang C, Kan JR. Magnetic merging line and reconnection voltage versus IMF clock angle: Results from global MHD simulations. Journal of Geophysical Research. 2009;**114**:08220. DOI: 10.1029/2009JA014118

IntechOpen